*V. Troshchenko**

High-Cycle Fatigue and Inelasticity of Metals

REFERENCE Troshchenko, V., **High-cycle fatigue and inelasticity of metals,** *Multiaxial and Fatigue Design*, ESIS 21 (Edited by A. Pineau, G. Cailletaud, and T. C. Lindley) 1996, Mechanical Engineering Publications, London, pp. 335–348.

ABSTRACT A method for the investigation of high-cycle fatigue and inelasticity of metals under conditions of symmetric cyclic loading in tension–compression, bending and torsion is described. A procedure for the calculation of true stresses and inelastic cyclic strains in surface layers under nonuniform stress conditions (bending, torsion) is proposed. A large group of steels has been studied and it is shown that the use of inelastic cyclic strains at the stage of stabilization of the deformation process as a measure of the fatigue damage accumulation intensity makes it possible to explain some general laws of high-cycle fatigue, including the influence of stress gradient and load biaxiality on the fatigue behaviour.

1 Introduction

In the present paper inelasticity is treated as a material property which manifests itself in a nonlinear relation between stresses and strains that leads to the formation of a closed hysteresis loop in the stress–strain coordinates under cyclic loading.

The main characteristics of inelasticity are inelastic cyclic strains (the hysteresis loop width) and the energy dissipated in a cycle (the hysteresis loop area). The effects which show up at inelastic deformation (decaying of vibrations, heating of specimens, etc.) have long been related to high-cycle fatigue (**1**, **2**, **3**). The drawback of these investigations is that they are incomplete, conducted generally under linear uniform stress conditions, and in the cases when the tests are performed on nonuniformly stressed specimens, averaged characteristics are determined.

This paper presents the results of a comprehensive study of interrelation between high-cycle fatigue and inelasticity of a large group of steels tested in tension–compression, bending and torsion by a unified method using thin-walled and solid specimens, as well as their analysis performed using true values of stresses and inelastic strains.

Special attention has been paid to the influence of nonuniform stress state (stress gradient) and load biaxiality.

*Institute for Problems of Strength, National Academy of Sciences of Ukraine, 2 Timiryazevskaya Str., Kiev 252014, Ukraine.

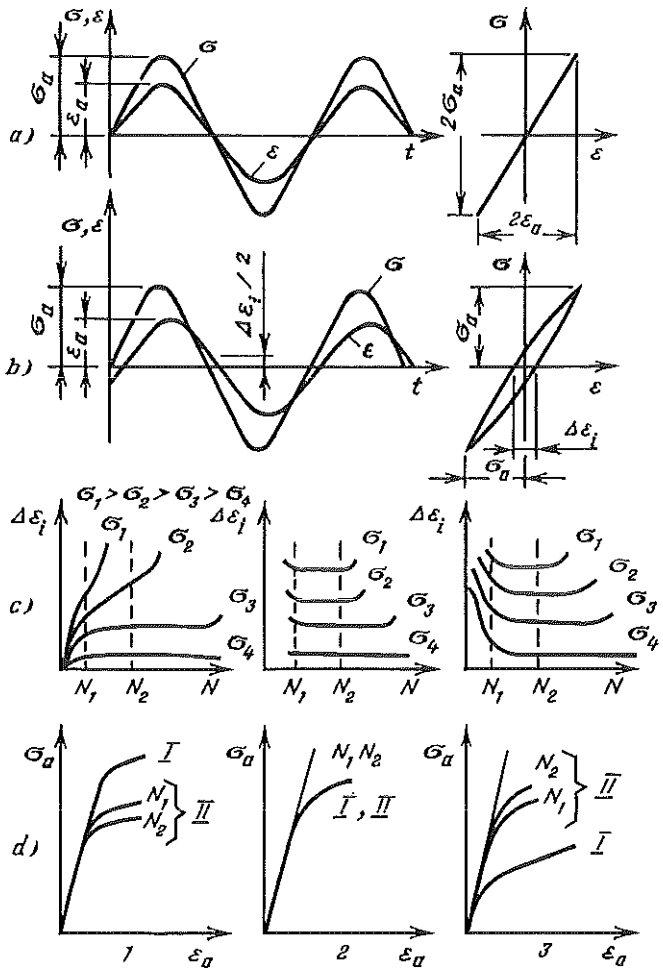

Fig 1 Variation of stress and strain signals with time for (a) elastic loading; (b) inelastic loading; (c) variation of the inelastic strain with the number of cycles for cyclic softening (1), cyclically stable (2) and cyclically hardening materials (3); (d) associated cyclic stress–strain curves.

2 Experimental Procedure

Inelasticity of metals gives rise to different effects. One of them is a shift of stress σ and strain ε signals. In the case of the material elastic deformation (Fig. 1a), a linear relation between stresses and strains is observed. When the material deforms inelastically (Fig. 1b), a closed hysteresis loop will be obtained whose width is equal to the inelastic strain in a cycle, $\Delta\varepsilon_i$, ($\Delta\gamma_i$ for a thin-walled specimen in torsion), and the area of the energy dissipated irreversibly in a cycle ΔW.

The hysteresis loop width may change depending on the number of load cycles. Figure 1c shows this variation for cyclically softening (1), cyclically stable (2) and cyclically hardening (3) materials tested under conditions when the load is maintained constant during the test (**4**).

Knowing the magnitude of inelastic strain in a cycle, one can plot a cyclic stress–strain diagram in the coordinates 'stress amplitude, σ_a, – strain amplitude, ε_a'

$$\varepsilon_a = \sigma_a/E + \Delta\varepsilon_i/2 \tag{1}$$

where E is the material elasticity modulus, σ_a is the normal stress amplitude.

Initial portions of static (I) and cyclic (II) stress–strain diagrams for different number of load cycles are given in Fig. 1d for materials of different classes.

The major part of the investigations was performed using a specially designed test system with a computer-controlled loading regime and processing of results (**4**). The system performed high-frequency scanning of the stress and strain signals and determined the magnitudes of the signals. The analysis made revealed that with such a principle of measurement and the corresponding apparatus one can measure inelastic strains as small as 5×10^{-6}.

In some cases the hysteresis loop was displayed directly on the screen of the oscilloscope.

The tests in tension–compression were carried out on cylindrical specimens of 5 mm diameter, in bending on specimens of 5 mm × 10 mm rectangular cross-section, in torsion on cylindrical specimens with an outer diameter of 14 mm, and inner diameter of 12 mm for thin-walled specimens.

Realization of each type of testing introduces its own special features into the processing of the results obtained.

2.1 *Tension–compression*

In tension–compression tests a device was used which allows the specimen strain measurement from the deformation of elastic elements fixed on the thicker parts of the specimen with the bending strains eliminated. Stresses were measured from the gauge readings on the dynamometer (**4**).

Inelastic strains were calculated by the following formula

$$\Delta\varepsilon_i = \frac{\sigma_a(1 + \beta_1)}{E(1/\beta - 1/2)} \tag{2}$$

where β is the ratio of the signals proportional to the hysteresis loop width and the strain amplitude ($\beta = \Delta x/x_a$); β_1 is the parameter which takes into account the deformation of the grips and the thickened parts of the specimens ($\beta_1 = 0.5 \ldots 0.8$).

The energy dissipated in a cycle is equal to

$$\Delta W = K\sigma_a\Delta\varepsilon_1 \tag{3}$$

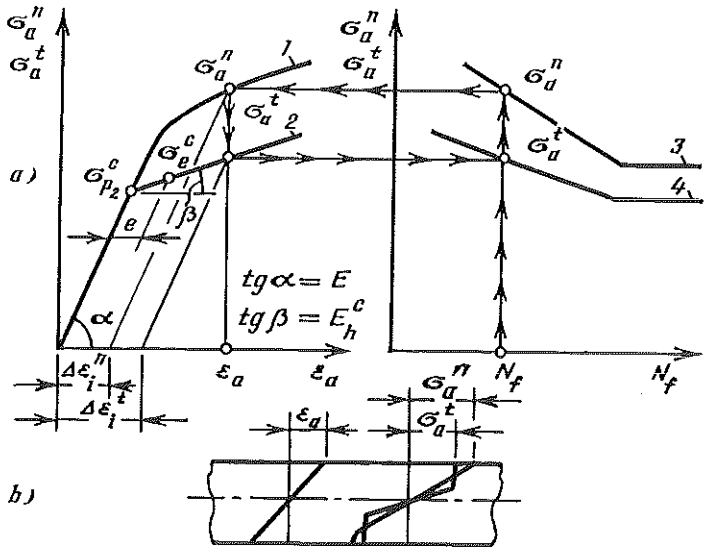

Fig 2 Schematic of plotting true stress–strain diagrams and fatigue curves.

where K is the coefficient of the hysteresis loop shape. Its value is close to $K = 1.33$.

2.2 *Bending*

In bending tests strains were measured directly on the specimen surface using a special-purpose high resolution gauge (5). The bending moment in the specified section was measured from the gauge readings on the dynamometer.

A feature of bending tests is that a hysteresis loop and, accordingly, a cyclic stress–strain diagram are obtained in the coordinates 'normal stress, σ_a^n, – strain in the material surface layer, ε_a'

$$\sigma_a^n = M_b/W$$

where M_b is the bending moment, W is the section inertia modulus.

The hysteresis loop width in the $\sigma_a^n - \varepsilon_a$ coordinates can be defined by the following formula

$$\Delta\varepsilon_i^n = \frac{\sigma_a^n}{E(1/\beta - 1/2)}$$

To calculate true stresses, σ_a^t, that is the stresses on the specimen surface which take into account the elastoplastic deformation (Fig. 2b), and the corresponding true values of inelastic strains, $\Delta\varepsilon_a^t$, a scheme was used as shown in Fig. 2a.

In this figure, 1 is the cylic stress–strain curve in the coordinates $\sigma_a^n - \varepsilon_a$ obtained experimentally, 2 is the true cyclic stress–strain diagram for the material surface layer in the coordinates $\sigma_a^t - \varepsilon_a$. In plotting line 2 it was assumed that its initial portion is a straight line.

Considering this assumption, the expression for stresses σ_a^n with the known values of ε_a and parameters $\varepsilon_{pr}^c(\varepsilon_{pr}^c = \sigma_{pr}^c/E)$ and E_h^c of the true stress–strain diagram (Fig. 2a) will have the following form (**6**)

$$\sigma_a^n = \frac{1}{\varepsilon_a^2}\left[E_h^c \varepsilon_a^3 + (E - E_h^c)(3\varepsilon_a^2 - \varepsilon_{pr}^{c^2})\frac{\varepsilon_{pr}^c}{2}\right] \tag{4}$$

Equation (4) has been obtained from the condition of bending moments equality assuming elastic and elastoplastic deformation of the material. Writing equation (4) for two points on Fig. 2 line 1 and solving this system of equations for ε_{pr}^c and E_h^c, we shall have the parameters needed to construct line 2.

The analysis performed (**4**) revealed that the error of ε_{pr}^c and E_h^c assessment, with some recommendations being observed, does not exceed 5%.

With a true stress–strain diagram and tolerances for residual strain e given (Fig. 2a), one can determine cyclic elasticity limits σ_c^c corresponding to these tolerances, as well as σ_a^t and $\Delta\varepsilon_i^t$.

With stress–strain lines 1 and 2 (Fig. 2a) and experimental fatigue curve 3 with coordinates $\sigma_a^n - \lg N_f$ it is possible to plot fatigue curve 4 with coordinates $\sigma_a^t - \lg N_f$ as shown in Fig. 2.

It is also possible to solve an inverse problem, where a stress–strain diagram with coordinates $\sigma_a^n - \varepsilon_a$ and a corresponding fatigue curve are plotted from the known true stress–strain diagram obtained in tension–compression with no account taken of the specific influence of the stress gradient.

2.3 *Torsion*

In torsion tests a twist angle was measured at the outer surface of the specimen. The torque was measured from the gauge readings on the dynamometer (**4**).

When testing thin-walled specimens the following calculations were used.

$$\Delta\gamma_i = \frac{\tau_a(1 + \beta_1)}{G(1/\beta - 1/2)} \qquad \tau_a = M_T/2bq$$

$$\gamma_a = \tau_a/G + \Delta\gamma_i/2 \qquad \Delta W = K\tau_a\Delta\gamma_i \tag{5}$$

where $\Delta\gamma_i$, γ_a are the inelastic part and the amplitude of relative shear of the specimen surface layer, respectively; M_T is the torque; q is the specimen wall thickness; b is the area enveloped by the median line of the thin-wall section; β, β_1 are the parameters similar to those mentioned earlier; G is the shear modulus.

When testing solid specimens in torsion, as well as in bending, a necessity arises of calculating true stresses and true inelastic cyclic strains.

The calculation procedure for this case is similar to that for bending (Fig. 2) if in this figure we substitute normal stresses by shear stresses and relative elongation by relative shear.

In this case the main formula will have the form

$$\Delta\gamma_i^n = \frac{\tau_a^n(1+\beta_1)}{G(1/\beta - 1/2)}, \qquad \tau_a^n = M_T W_p$$

where W_p is the polar section inertia modulus.

The relationship for nominal stresses obtained on the basis of the same approach as equation (4) was taken in the following form

$$\tau_a^n = \gamma_{pr}^c G\left[\frac{\gamma_a}{\gamma_{pr}^c} + \frac{4}{3}\left(1 - \frac{G_h^c}{G}\right)\left(1 - \frac{1}{4}\frac{1}{(\gamma/\gamma_{pz}^c)}\right)^3\right] \tag{6}$$

where γ_{pr}^c and G_h^c are the strain corresponding to the proportionality limit and the hardening modulus on the true cyclic stress–strain diagram, respectively.

High-cycle fatigue tests were performed with a symmetric cycle and the loading regimes which ensured constant values of σ_a (tension–compression), σ_a^n (bending), τ_a (torsion of a thin-walled specimen), τ_a^n (torsion of a solid specimen). Unless otherwise specified, fracture criterion was taken to be the initiation of a crack several millimetres in size.

Fatigue curves were plotted on the test basis of 10^7 cycles. The loading frequency was between 20 and 40 Hz.

2.4 *Materials*

The investigations were performed on carbon and low-alloy steels subjected to different thermal treatments. These steels are widely used in engineering for manufacturing components operating under high-cycle loading.

Mechanical properties of the steels studied are listed in Table 1. They are all cyclically softening materials. Specimens were fabricated using the regimes which provided for the minimum residual stresses on the surface and a high level of surface finish.

Table 1 Mechanical properties of the steels

Steel	*Thermal treatment*	*Yield strength 0.2%* $\sigma_{0.2}$ (MPa)	*Ultimate tensile strength* σ_u (MPa)	*Elongation* δ (%)	*Reduction of area* ψ (%)
15kp	as-received	267	413	40.1	68.9
45 (I)	as-received	468	716	22.8	46.9
45 (II)	as-received	339	516	33.4	66.0
45 (III)	normalized at 1103 K for 0.5 hr	476	668	32.0	48.0
15G2AFDps	as-received	410	532	32.3	72.0

1Kh17N2Sh	oil-quenched at 1263 K for 2 hr, tempered at 832 K in water for 2 hr	664	869	17.8	58.1
12KhN3A	normalized at 1133 K, quenched at 1073 K, tempered at 453 K	700	950	11.0	55.0
40Kh (I)	quenched at 1133 K, tempered at 923 K	683	803	22.5	70.2
40Kh (II)	oil-quenched at 1133 K for 0.5 hr, tempered at 1023 K in air	675	840	20.0	67.0
40Kh (III)	water-quenched at 1133 K for 0.5 hr, tempered at 923 K in air	590	853	25.0	58.0
1Kh13	air-quenched at 1273 K fr 2 hr, tempered at 1033 K in air	614	746	20.0	64.0
EI-612 (I)	water-quenched at 1303 K, aged at 1123 ... 1173 K for 10 hr followed by further aging at 973 ... 983 K for 25–50 hr	582	896	26.0	36.0
EI-612 (II)	water-quenched at 1303 K for 1 hr, aged at 973 K for 25.5 hr in air	595	1000	24.0	36.6

3 Interrelation Between High-Cycle Fatigue and Inelasticity of Metals

3.1 *Fatigue endurance curves and inelastic strains*

Typical $\Delta\varepsilon_i$ vs N relations and corresponding cyclic stress–strain diagrams $\sigma_a - \varepsilon_a$ are given in Fig. 1c.

The analysis involved inelastic strains corresponding to the stage of stabilization or to $0.5N_f$.

Figure 3 shows fatigue curves for steels 15kp and 45 (I) tested in tension–compression with conventional coordinates $\sigma_a - \log N_f$ (a) and with coordinates $\log \Delta\varepsilon_i - \log N_f$ (b). Similar symbols in these figures correspond to similar test conditions.

This figure reveals that plotting the fatigue curves with coordinates $\log \Delta\varepsilon_1 - \log N_f$ lowers appreciably the scatter of the test results. This indicates that inelastic strains account not only for the level of the external loading, but also for the capacity of the material, individual specimens included, to resist the action of external forces.

Figure 4 presents initial portions of cyclic stress–strain diagrams 1 and high-cycle fatigue curves 2 for thin-walled specimens of steels in torsion and in tension–compression.

This figure, which is a typical one, shows that the fatigue limits for steels correspond to the region of transition from elastic to inelastic deformation irrespective of mechanical properties and type of loading (torsion, tension–compression).

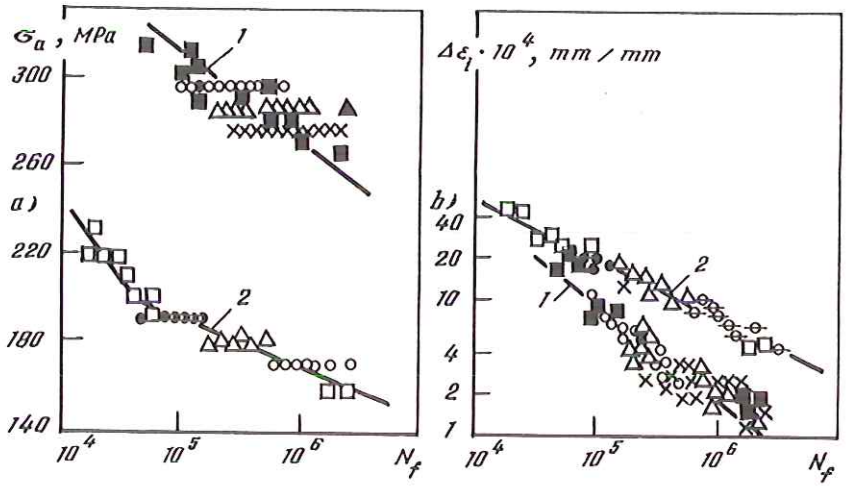

Fig 3 Fatigue curves for steels 45 (I) curve (1) and 15kp curve (2).

3.2 *Stress gradient*

The influence of stress gradient on high-cycle fatigue and inelastic cyclic strains was analysed from the results obtained in tension–compression (relative gradient $\bar{\eta} = 0$), in bending ($\bar{\eta} = \frac{2}{h} = 0.2\ \text{mm}^{-1}$, where h is the specimen height) and in torsion of thin-walled and solid specimens ($\bar{\eta} = \frac{2}{d} = \frac{1}{7}$, d is the specimen diameter) (**5, 7**).

Figure 5 shows fatigue curves in tension–compression with coordinates $\sigma_a - \lg N_f$ curve 1 and in bending with coordinates $\sigma_a^n - \log N_f$ curve 2 for steels 15G2AFDps (a), 45(III) (b), 1Kh13 (c), 1Kh13(II) (d) and EI–612(I) (e).

Dashed lines 3 in this figure represent fatigue curves with coordinates $\sigma_a^n - \lg N_f$ calculated using the procedure given in Fig. 2 (inverse problem). These curves were constructed using the experimental cyclic stress–strain diagram, the fatigue curve for tension–compression and equation (4).

From Fig. 5 it follows that only for steels 15G2AFDps and 45 (III) the difference between fatigue curves for tension–compression 1 and for bending 2 is associated with the difference between nominal and true stresses. For the rest of the steels the distinction between the fatigue curves cannot be explained by this fact alone, which means that the effect of the stress gradient is important.

This effect can be explained by the fact that under nonuniform stress conditions the process of the material surface layer softening under cyclic loading, which is responsible for the difference between the static and cyclic stress–strain diagrams, is much influenced by less stressed inner layers of the material. These layers retard the initiation of inelastic strains on the surface. This is confirmed by the results listed in Table 2 which compares cyclic elasticity limits σ_e^c and fatigue limits in tension–compression σ_{-1} and in bending $(\sigma_e^c)_b$, $(\sigma_{-1})_b$ at similar

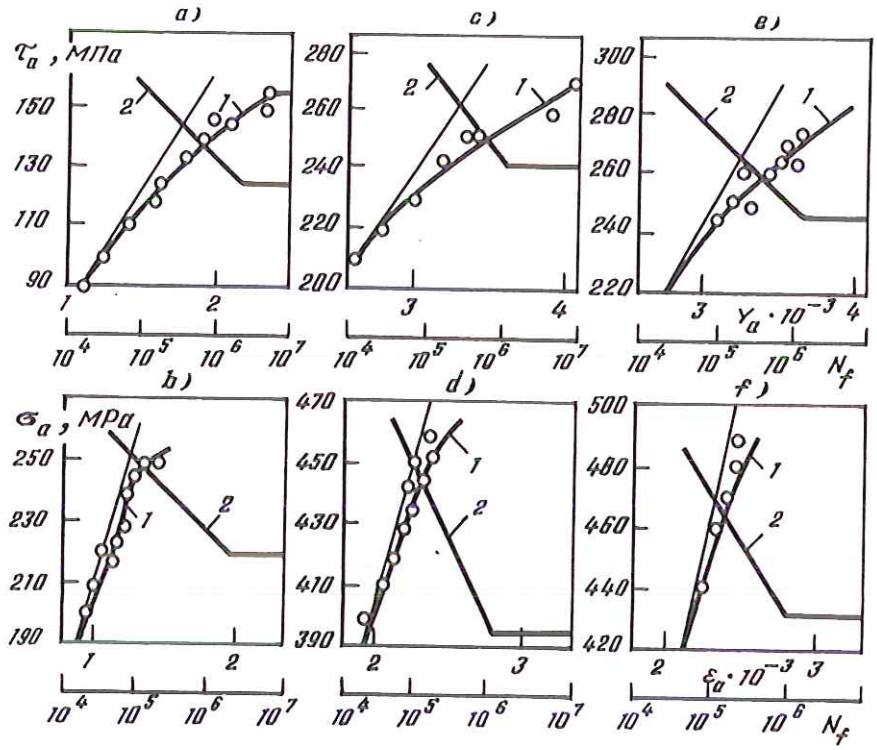

Fig 4 Initial portions of stress–strain curves (1) and fatigue curves (2) for steels 45 (II) (a, b), 12KhN3A (c, d) and 40Kh (I) (e, f).

tolerances for inelastic strain at stresses equal to the fatigue limit $(\Delta\varepsilon_i)_{\sigma_{-1}}$.

Cyclic elasticity limits in bending were determined from true stress–strain diagrams computed by the procedure described above.

The magnitude of inelastic strain in a cycle can be taken as the value defining the number of cycles to fracture and independent of the stress gradient. Steel 15G2AFDps is an exception, which might be related to the fact that this material was sensitive to self-heating during cyclic loading.

Table 2 Relationship between fatigue limits and cyclic elasticity limits

Steel	*Tension-compression*			*Bending*	
	σ_{-1} (MPa)	$(\Delta\varepsilon_i)_{\sigma_{-1}} \times 10$ (mm/mm)	σ_ε^c (MPa)	$(\sigma_{-1})_b$ (MPa)	$(\sigma_\varepsilon^c)_b$ (MPa)
15G2AFDps	250	23	240	300	275
45 (III)	260	25	243	305	285
1Kh13	250	0.7	385	400	432
EI-612 (I)	260	0.35	275	310	336

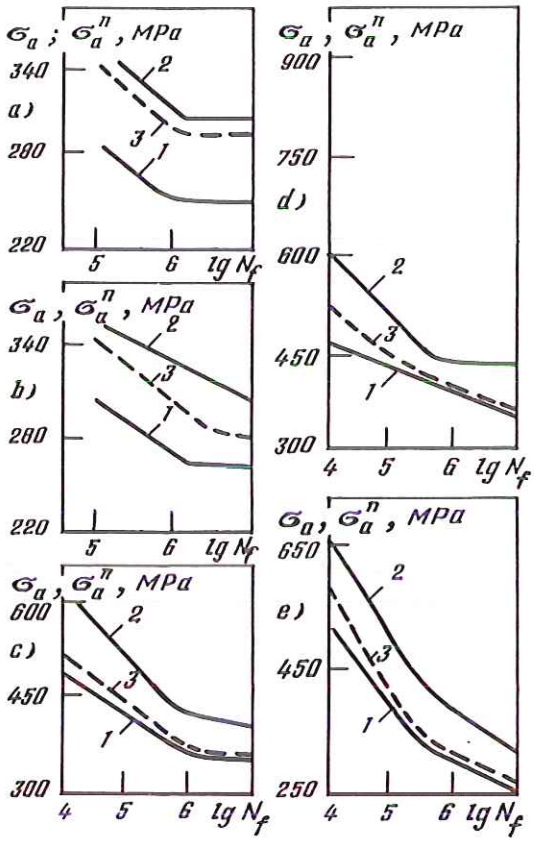

Fig 5 Experimental and calculated fatigue curves.

The influence of the stress gradient upon high-cycle fatigue in torsion can be illustrated by the results presented in Table 3, where τ_{-1}, τ^t_{-1} and τ^n_{-1} are fatigue limits of thin-walled and solid specimens in terms of true and nominal stresses, respectively; τ^c_{pr} is the proportionality limit determined by the method described above.

Table 3 Comparison of fatigue limits in torsion

Steel	T (K)	τ_{-1} (MPa)	τ^t_{-1} (MPa)	τ^n_{-1} (MPa)	τ^c_{pr} (MPa)
40Kh (III)	293	205	205	235	200
1KhPN2Sh	293	295	295	305	—
EI–612 (II)	293	180	215	235	209
EI–612 (II)	893	165	225	240	201

From Table 3 it follows that while for steels 40Kh(III) and 1Kh17N2Sh the influence of stress gradient is insignificant (as witnessed by the equality of τ_{-1} and τ^{t}_{-1}) for steel EI–612 at room and high temperatures the magnitude of τ^{t}_{-1} is much higher than that of τ_{-1}.

3.3 *Load biaxiality*

Considering the results presented above, when analysing the influence of load biaxiality or multiaxiality one should take into account a possible contribution of the stress gradient. With this in view, the influence biaxiality was analysed from the test results obtained in tension–compression and in bending of thin-walled specimens.

Table 4 presents the expressions for reduced stresses according to the theories of normal strains (II), shear stresses (III), von Mises energy (IV), as well as octahedral stresses and corresponding strains. In these formulae E′ and G′ are the secant moduli defined from the experimentally plotted diagrams σ_a vs ε_a, τ_a vs γ_a (Fig. 4), μ' is the coefficient determined from the following formula (**9**):

$$\mu' = 0.5 - \frac{\sigma_t}{E_e}(0.5 - \mu)$$

where μ is the Poisson ratio ($\mu = 0.25$), σ_t and e are true stresses and strains, respectively.

Table 4 Reduced stresses and strains

Type of loading	*Relations for reduced stresses and strains*			
	II	III	IV	Octahedral stresses and strains
Tension	$\sigma_{II} = \sigma_a$	$\sigma_{III} = \sigma_a/2$	$\sigma_{IV} = \sigma_a$	$\tau_{oct} = \frac{\sqrt{2}}{3}\sigma_a$
	$\varepsilon_{II} = \varepsilon_a$	$\gamma_{III} = \frac{\sigma_a}{E'}(1 + \mu')$	$\varepsilon_{IV} = \varepsilon_a$	$\tau_{oct} = \frac{\sigma_a 2\sqrt{2}(1 + \mu')}{3E'}$
Torsion	$\sigma_{II} = \tau_a(1 + \mu')$	$\sigma_{III} = \tau_a$	$\sigma_{IV} = \sqrt{3}\tau_a$	$\tau_{oct} = \sqrt{\frac{2}{3}}\tau_a$
	$\varepsilon_{II} = \gamma_a/2$	$\varepsilon_{III} = \gamma_a$	$\varepsilon_{IV} = \frac{\sqrt{3}\tau_a}{G'(1 + \mu')}$	$\tau_{oct} = \sqrt{\frac{2}{3}}\frac{\tau_a}{G'}$

Figure 6 presents initial portions of cyclic stress–strain diagrams for steel 45(II) plotted using the expressions from Table 4 and stress–strain diagrams for tension–compression curve 2 and torsion curve 1. Similar results were also obtained for steels 12KhN3A and 40Kh(I). This suggests that the process inelastic deformation is governed by octahedral stresses and strains.

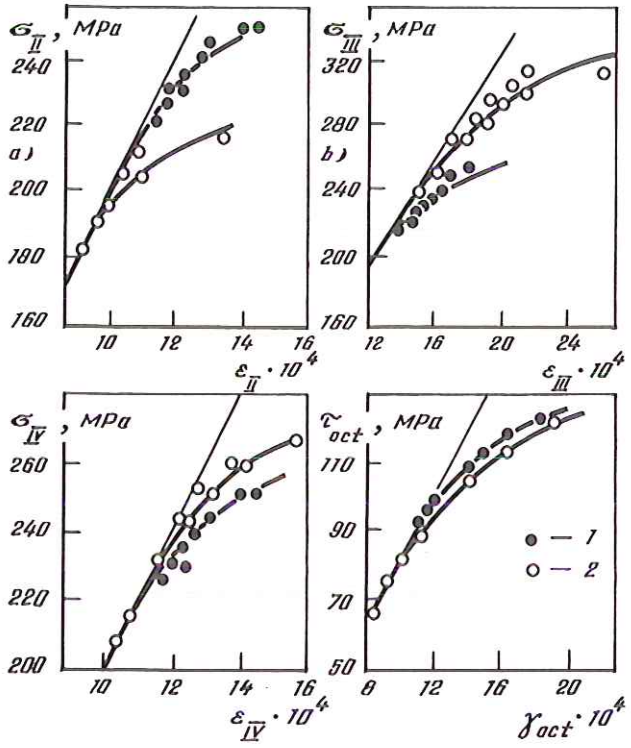

Fig 6 Initial portions of cyclic stress–strain diagrams for steel 45 (II).

Figure 7 shows fatigue curves for tension–compression curve 2 and torsion of thin-walled specimens curve 1 of the material studied, which are plotted for the number of load cycles to the initiation of surface cracks the size 0.1 mm (light points) and to final fracture (dark points).

In Fig. 7 it is observed that the experimental points obtained in tension–compression and in torsion fall on single fatigue curves with coordinates τ_{oct} vs lg N_f. The best agreement is observed for the fatigue curves plotted in terms of crack initiation.

From the results presented above it follows that the ratio of fatigue limits obtained in torsion of thin-walled specimens and in tension–compression corresponds to $\tau_{oct}/\sigma_{-1} = 0.577$. In the case where the analysis of the load biaxiality effect involves also the results of testing in bending (linear stress state) and in torsion of solid specimens (biaxial stress state), one can obtain a large scatter of results. For the investigated steels the τ_{-1}/σ_{-1} ratio was within the limits 0.45 ... 0.83.

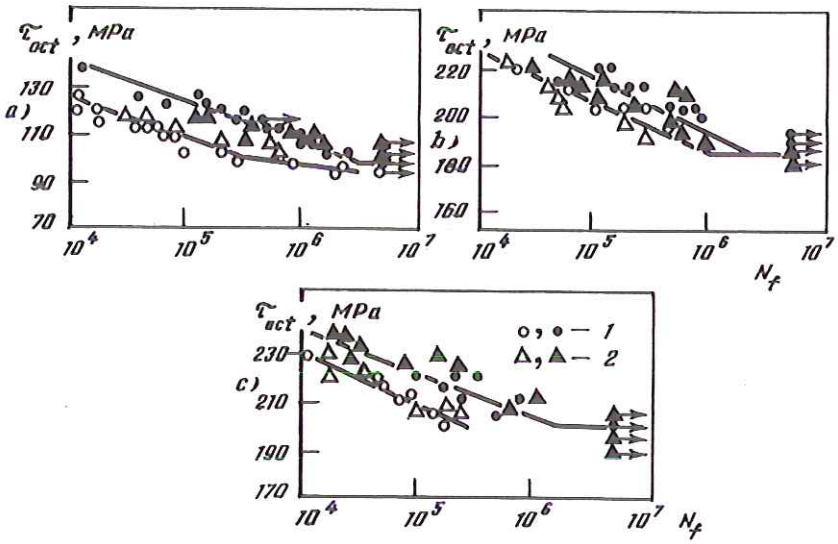

Fig 7 Fatigue curves for steels 45 (III) (a), 12KhN3A (b), and 40Kh (I) (c).

4 Conclusions

A method for the investigation of inelastic cyclic strains during high-cycle fatigue in tension–compression, bending and torsion is proposed and substantiated. Special attention is paid to the justification of the determination of true inelastic cyclic strains under nonuniform stress conditions (bending, torsion).

High-cycle fatigue and inelasticity of a number of carbon and low-alloy steels has been studied and it is shown that the use of cyclic inelastic strains at the stage of stabilization of the deformation process as a measure of the intensity of fatigue damage accumulation at high-cycle fatigue makes it possible to take into account the changes in the material properties during cyclic loading and the influence on these changes of such factors as nonuniform stress state (stress gradient) and load biaxiality, to consider the scatter of the test results, to relate the fatigue limit and the number of cycles to fracture and the level of inelastic cyclic strains.

Significant influence of the stress gradient on the process of surface layer deformation in bending and in torsion has been revealed which results in an increase of the cyclic proportionality and elasticity limits of these layers as compared to tension–compression and torsion of thin-walled specimens of the same materials. A correlation has been established between fatigue limits and cycle elasticity (proportionality) limits in tension–compression, bending and torsion.

It is shown that cyclic stress–strain diagrams for the steels investigated in tension–compression and in torsion of thin-walled specimens can be represented by a single curve in the $\tau_{oct} - \gamma_{oct}$ coordinates.

The results of the investigation of high-cycle fatigue under tension–compression and torsion reveal the coincidence of fatigue curves with the coordinates 'octahedral stress – number of cycles to crack initiation (final fracture)'. With this in view the ratio of fatigue limits in torsion and in tension–compression is equal to 0.577. It is shown that this ratio can be essentially different if the analysis is based on the fatigue limits for a solid specimen in bending or in torsion when the influence of stress gradient takes place.

References

(1) LAZAN, B. J. (1950) A study with new equipment of the effects of fatigue stress on the damping capacity and elasticity of mild steel, *Trans. Amer. Soc. Mat.*, **42**, pp. 499–558.
(2) HANSTOCK, R. F. (1947) Damping capacity, strain hardening and fatigue, *Proc. Phys. Soc.*, **59**, pp. 275–287.
(3) FELTNER, G. E. and MORROW, J. D. (1961) Microplastic strain hysteresis energy as a criterion for fatigue fracture, *Trans. ASME(D)*, **81**, N.1.
(4) TROSHCHENKO, V. T. (1981) *Deformation and Fracture of Metals under High-cycle Loading* (in Russian), Naukova Dumka, Kiev.
(5) TROSHCHENKO, V. T. and ZHABKO, N. I. (1981) Deformation and fracture of metals subjected to high-cycle loading under nonuniform stress condition (in Russian), *Problemy Prochnosti*. **9**, pp. 3–11, **11**, pp. 3–10.
(6) IVANOV, G. T. and SKORYI, I. A. (1959) On the problem of the stress vs strain diagram approximation, in: *Problems of Strength of Materials* (in Russian). Oborongiz, 13–32.
(7) TROSHCHENKO, V. T., KHAMAZA, L. A., NIKOLAEV, I. A. and DRAGAN, V. I. (1984) Strain criteria of fatigue fracture which take into account the type of stress state (in Russian), *Problemy Prochnosti*, **1**, pp. 6–10.
(8) TROSHCHENKO, V. T. and MITCHENKO, E. I. (1984) Lifetime prediction at program cyclic loading considering property dissipation (in Russian), *Problemy Prochnosti*, **10**, pp. 3–8.
(9) CHERNYAK, N. I. (1962) *Mechanical Properties of Steel in a Low Plastic Strain Region* (in Russian), Izdatel'stvo AN Ukr. SSR, 103.